

Hammad A. Faizi¹ 
 Rumiana Dimova² 
 Petia M. Vlahovska³ 

¹Department of Mechanical Engineering, Northwestern University, Evanston, IL, USA

²Department of Theory and Biosystems, Max Planck Institute of Colloids and Interfaces, Science Park Golm, Potsdam, Germany

³Department of Engineering Sciences and Applied Mathematics, Northwestern University, Evanston, IL, USA

Received April 3, 2021

Revised July 1, 2021

Accepted July 9, 2021

Research Paper

Electromechanical characterization of biomimetic membranes using electrodeformation of vesicles

We describe a facile method to simultaneously measure the bending rigidity and capacitance of biomimetic lipid bilayers. Our approach utilizes the ellipsoidal deformation of quasi-spherical giant unilamellar vesicles induced by a uniform AC electric field. Vesicle shape depends on the electric field frequency and amplitude. Membrane bending rigidity can be obtained from the variation of the vesicle elongation on either field amplitude at fixed frequency or frequency at fixed field amplitude. Membrane capacitance is determined from the frequency at which the vesicle shape changes from prolate to oblate ellipsoid as the frequency is increased at a given field amplitude.

Keywords:

Bending rigidity / Electrodeformation / Lipid bilayers / Membrane capacitance
 DOI 10.1002/elps.202100091

1 Introduction

Cells and their internal organelles are enveloped by thin sheets made of lipid bilayers. Mechanical properties of these lipid membrane such as the bending rigidity regulate many cell biological processes, for example, membrane fusion and fission [1], mechanosensing [2–4], and cell motility [5, 6], to name a few. An electric potential difference across the plasma membrane exists in living cells, and electrical properties such as capacitance play crucial role in the propagation of action potentials in neurons [7, 8], electromotility of outer hair cells in hearing [9], and cardiomyocyte contractions in heart beating [10].

An *in vitro* membrane system, such as the giant unilamellar vesicle (GUV), which is a cell-sized sac of closed lipid bilayer (typical radius of 10 μm), provides a well-defined model to assay membrane properties and investigate the electromechanics of membranes at a fundamental level [11–13]. Several experimental methods are widely used to measure bending rigidity and tension using GUVs [14]. Fluctuation spectroscopy analyzes the thermally driven membrane undulations with micron and submicron wavelength recorded with optical microscopy [15–21]. Tension and bending rigidity control the dynamics of the long and short wavelength undulations, respectively. The method works best if membrane tension is very low ~10⁻⁹ N/m in order to resolve enough wavelengths for good statistics. GUVs can be analyzed by micropipette aspiration [22, 23] and electrodeformation [18, 24, 25]. These methods analyze

macroscale vesicle deformation (on the scale of the vesicle radius) induced by either pressure or electric field. The latter approach is particularly appealing because of its easy implementation and versatility—in addition to membrane elastic properties, it can be utilized to obtain membrane capacitance [26] and viscosity [27, 28].

In this paper, we provide the theoretical foundations of the electrodeformation method and show how to utilize it to simultaneously measure bending rigidity, tension and capacitance of lipid bilayer membranes.

2 Materials and methods

2.1 The electrodeformation method

The method relies on the entropic elasticity of lipid bilayers. Lipid bilayers are very soft and thermal fluctuations cause membrane undulations that store area. Application of electric stress causes vesicle deformation and the vesicle apparent area A increases due to flattening of the thermally driven suboptimal membrane undulations; see Fig. 1.

Restricting the fluctuations raises the membrane tension [22, 29]:

$$\sigma = \sigma_0 \exp \left[\frac{8\pi\kappa}{k_B T} \alpha \right], \quad \alpha = \frac{A - A_0}{A_0}, \quad (1)$$

where σ_0 and $A_0 = 4\pi R^2$ are the membrane tension and vesicle area in absence of applied stress, respectively. 1 can be used to obtain the membrane bending rigidity κ if the area increase and tension can be measured independently. Next, we show how the tension can be calculated from the applied electric field.

Color online: See article online to view Figs. 2 and 4–6 in color.

Correspondence: Dr. Petia M. Vlahovska, Department of Engineering Sciences and Applied Mathematics, Northwestern University, Evanston, IL 60208, USA.

E-mail: petia.vlahovska@northwestern.edu

Abbreviation: GUV, giant unilamellar vesicle

2.2 Theoretical model of vesicle electrodeformation

Let us consider a vesicle made of a charge-free lipid bilayer membrane with bending rigidity κ , tension σ , capacitance C_m . The vesicle is suspended in a solution with conductivity λ_{ex} and permittivity ε_{ex} , and filled with a different solution characterized by λ_{in} and ε_{in} .

A uniform AC electric field with amplitude E_0 and frequency ω , $\mathbf{E} = E_0 \cos(\omega t) \hat{\mathbf{z}}$, deforms the vesicle into a spheroid with symmetry axis aligned with the field direction. The spheroid aspect ratio is $v = a/b$, where a is the length of the symmetry axis and b is the length of the axis perpendicular to the symmetry axis, see sketch in Fig. 1. For small deformations, $v \lesssim 1.3$, the shape is well approximated by

$$r_s(\theta) = R \left(1 + \frac{s}{2} (1 + 3 \cos 2\theta) \right), \quad (2)$$

where r_s is the position of the surface, R is the initial radius of the vesicle, s is the deformation parameter, and θ is the angle with the applied field direction; $\theta = 0$ and $\pi/2$ correspond to the pole and the equator, respectively. The ellipsoid aspect ratio is related to the deformation parameter by $v = (1+s)/(1-2s)$. The theory developed by Vlahovska et al. [25, 30–32] predicts that the steady deformation parameter is given by the balance of electric and membrane stresses:

$$s = \varepsilon_{\text{ex}} E_0^2 R^3 \frac{p^{\text{el}}(\omega)}{6\kappa + \sigma R^2}. \quad (3)$$

The frequency dependence of the electric stress is given by

$$p^{\text{el}} = \frac{1}{48} (4(1 - P_{\text{ex}}^r) + P_{\text{ex}}^2 - 4SP_{\text{in}}^2), \quad (4)$$

where

$$\begin{aligned} P_{\text{ex}} &= \frac{K_{\text{ex}} + K_{\text{in}}(V_m - 1)}{K_{\text{in}} + 2K_{\text{ex}}}, & P_{\text{in}} &= \frac{K_{\text{ex}}(3 - 2V_m)}{K_{\text{in}} + 2K_{\text{ex}}}, \\ V_m &= \frac{3K_{\text{in}}K_{\text{ex}}}{2K_{\text{in}}K_{\text{ex}} + iC_m(K_{\text{in}} + 2K_{\text{ex}})\bar{\omega}}. \end{aligned} \quad (5)$$

Here $\bar{\omega} = \omega\varepsilon_{\text{ex}}/\lambda_{\text{ex}}$ and $\bar{C}_m = C_m R/\varepsilon_{\text{ex}}$ are the dimensionless frequency and membrane capacitance. $K_{\text{in}} = 1 + i\bar{\omega}$ and $K_{\text{ex}} = \Lambda + i\bar{\omega}S$ are the dimensionless complex permittivities. $S = \varepsilon_{\text{in}}/\varepsilon_{\text{ex}}$ and $\Lambda = \lambda_{\text{in}}/\lambda_{\text{ex}}$ are the ratios of permittivities and conductivities of the fluids interior and exterior to the vesicle. P^r is the real part of P , and $P^2 = PP^*$, where the superscript * denotes complex conjugate.

Typically, both inner and outer fluids are aqueous solutions with similar permittivities, $\varepsilon_{\text{in}} \approx \varepsilon_{\text{ex}} = \varepsilon$, hence S can be set to 1. In this case, 3 reduces to

$$s(\bar{\omega}) = \frac{\varepsilon E_0^2 R^3}{\kappa(6 + \bar{\sigma})} \frac{3[\bar{\omega}^2(\bar{C}_m^2(\Lambda + 2)^2(\Lambda - 1)(\Lambda + 3) + 2\bar{C}_m\Lambda(\Lambda^2 + \Lambda - 2) + 9\Lambda^2) + \Lambda^2(\Lambda + 2)^2]}{16((\Lambda + 2)^2 + 9\bar{\omega}^2)(\bar{C}_m^2(\Lambda + 2)^2\bar{\omega}^2 + 4\Lambda^2)}, \quad (6)$$

where $\bar{\sigma} = \sigma R^2/\kappa$. For a given vesicle with specified Λ and C_m , the aspect ratio can be modulated by varying either

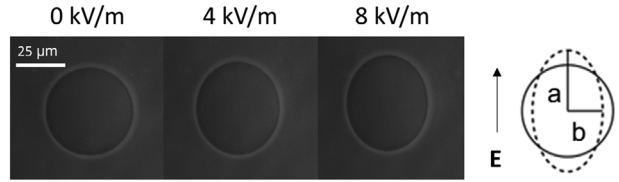


Figure 1. An initially spherical vesicle deforms into an ellipsoid and its apparent area increase when a uniform AC electric field is applied. The conductivity conditions inside and outside the vesicle correspond to $\lambda_{\text{in}} = 25 \mu\text{S}/\text{m}$ (0.2 mM NaCl) and $\lambda_{\text{ex}} = 3 \mu\text{S}/\text{m}$ (0 mM NaCl). The conductivity ratio is $\Lambda = 8.33$. The AC field frequency is 10 kHz. Images are obtained with phase contrast microscopy.

the electric field amplitude at fixed frequency or the field frequency at a given field strength. These two modalities of electrodeformation can be utilized to yield the vesicle electromechanical properties: bending rigidity, tension, and capacitance. The details of the implementation of the two approaches are discussed in Sections 3.1 and 3.2.

2.3 Vesicle preparation

GUVs are formed from the lipid palmitoyloleoylphosphatidylcholine, dipalmitoylphosphatidylcholine, and cholesterol, which are purchased from Avanti Polar Lipids (Alabaster, AL). The vesicles were produced using the electroformation method [33]. The stock solutions of 12 mM lipid in chloroform are diluted to 4 mM from which 8 μL of the solution is spread on the conductive sides of the indium tin oxide (ITO) slides (PGO, Germany). The slides are stored in vacuum for 2 h to evaporate all the organic solvents. The two slides are then sandwiched with a 2 mm thick Teflon spacer and the electroformation chamber is filled with 40 mM sucrose solution in 0.1–1 mM of NaCl. The chamber is connected to a signal generator (Agilent, USA) for 2 h at 50 Hz and from Teflon with two 92 μm cylindrical voltage 1.5 V_p (voltage amplitude). The harvested vesicles are diluted in isotonic glucose solution in 0.1–1 mM NaCl. Solutions conductivities were measured with S47 Mettler Toledo conductivity meter (USA).

2.4 Electrodeformation

The electrodeformation experiments are conducted in the electrofusion chamber (Eppendorf, Germany). The chamber is made from Teflon with two 92 μm cylindrical platinum parallel electrodes 500 μm apart. The field is applied using a

function generator (Agilent 3320A). The function generator is controlled using a custom built MATLAB (Mathworks, USA)

program. This gives a precise control over the strength and duration of applied electric fields.

2.5 Optical microscopy and imaging

The vesicles are visualized using a phase contrast microscope (A1 Axio Observer, Zeiss, Germany) with $63\times$ objective 0.75 NA (air). Imaging is performed using Photron SA1.1 camera. The image acquisition rate for electrodeformation recordings is kept to a constant of 60 fps for lipid vesicles and the shutter speed is fixed to $300\ \mu\text{s}$. The time evolution of the vesicle is analyzed using a homemade image analysis software. The software uses a Fourier series to fit around the vesicle contour, $r_s = \sum_{n=0}^{\infty} c_n \cos(n\theta) + d_n \sin(n\theta)$, where r_s is the vesicle contour radius at the azimuthal angle θ , c_n and d_n are the amplitude of the mode number n . The second mode in the series is used to determine the major and minor axis, a and b , of the deformed vesicles to evaluate $v = (1 + c_2)/(1 - c_2)$ [18, 20, 21].

3 Results and discussion

3.1 Tension-area strain curve from increasing field amplitude yields bending rigidity

If tension is much stronger than bending rigidity forces, $\bar{\sigma} \gg 1$, then we can use Eq. (3) to determine the tension as a function of area strain:

$$\sigma(s, E_0) = \frac{\varepsilon E_0^2 R p^{\text{el}}(\omega)}{s}. \quad (7)$$

In terms of the deformation parameter, the area strain $\alpha \approx 8s^2/5$ [34]. Substituting in Eq. (1), using the expressions in terms of the deformation parameter, we obtain

$$\ln \frac{\varepsilon R p^{\text{el}}(\omega)}{\sigma_0} + \ln \frac{E_0^2}{s} = \frac{8\pi\kappa}{k_B T} \left(\frac{8s^2}{5} \right). \quad (8)$$

The bending rigidity is thus determined from the slope of the linear fit of s^2 as a function of $\ln E_0^2/s$. Figure 2 illustrates the use of method.

In the original implementation [24], the tension was computed assuming low frequency ($\bar{\omega} \rightarrow 0$):

$$\sigma = \frac{9\varepsilon E_0^2 R}{16} (H(0) - H(\pi/2))^{-1}, \quad (9)$$

where $H(\theta)$ is the mean curvature of the ellipsoid

$$H(\theta) = \frac{a(a^2 + 3b^2 + (b^2 - a^2)\cos 2\theta)}{\sqrt{2b(a^2 + b^2 + (b^2 - a^2)\cos 2\theta)}^{3/2}}. \quad (10)$$

For small aspect ratios, in terms of the deformation parameter, $H(\theta) \approx 1 + s(1 + 3\cos 2\theta)$ and the above formula reduces to Eq. (3) with $\bar{\omega} = 0$. The area strain is computed from the aspect ratio and for a prolate ellipsoid ($v > 1$) it is

$$\alpha = \frac{1}{2} v^{-2/3} \left(1 + v \frac{\arcsin(e)}{e} \right), \quad e = \sqrt{1 - v^{-1/2}}. \quad (11)$$

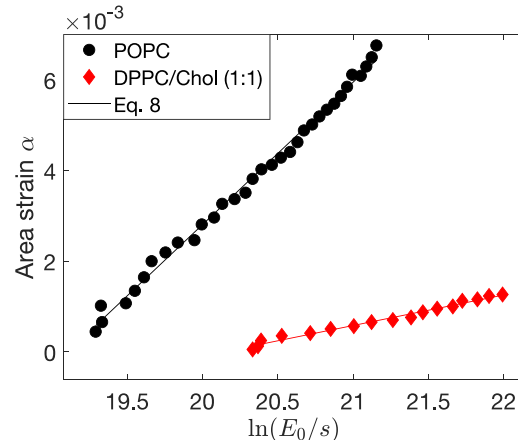


Figure 2. Area strain $\alpha = 8s^2/5$ versus $\ln(E_0^2/s)$ for palmitoyloleoylphosphatidylcholine (POPC) and dipalmitoylphosphatidylcholine/cholesterol (DPPC/Chol) (1:1) vesicle. For POPC, $R = 26\ \mu\text{m}$, $\lambda_{\text{in}} = 42\ \mu\text{S/m}$ (0.5 mM NaCl), and $\lambda_{\text{ex}} = 107\ \mu\text{S/m}$ (0.8 mM NaCl). Electric field amplitude was increased from 2 to 10 kV/m at increments of 0.25 kV/m. The AC field frequency is 0.2 kHz. The bending rigidity determined from the slope is $12.67\ k_B T$ and the tension obtained from the intercept is $1.76 \times 10^{-7}\ \text{N/m}$ with R -squared value of 0.994. For DPPC/Chol (1:1), $R = 21.2\ \mu\text{m}$, $\lambda_{\text{in}} = 3\ \mu\text{S/m}$ (0 mM NaCl), and $\lambda_{\text{ex}} = 120\ \mu\text{S/m}$ (1 mM NaCl). Electric field amplitude was increased from 2 to 10 kV/m at increments of 0.5 kV/m. The AC field frequency is 1 kHz. The bending rigidity determined from the slope is $58.01\ k_B T$ with R -squared value of 0.983.

Setting $a = 1 + s$ and $b = 1 - 2s$ and expanding for small s , recovers the area strain in terms of the deformation parameter, $\alpha \approx 8s^2/5$.

The electrodeformation method for measuring the bending rigidity was originally developed assuming low frequencies, $\bar{\omega} \rightarrow 0$. However, as seen from Eq. (8) the method can be performed at any frequency because the frequency-dependent prefactor $p^{\text{el}}(\omega)$ is absorbed in the intercept and does not affect the slope. Figure 3 shows that the bending rigidity is indeed independent of the frequency. Furthermore, the values for the bending rigidity in Fig. 3 and obtained from Fig. 2, which were done with different NaCl concentration in the suspending solution, are similar thus suggesting that the bending rigidity is insensitive to the salt conditions at such low concentrations.

3.2 Frequency-dependent vesicle shape yields capacitance and bending rigidity

Vesicle deformation depends not only on field strength but also on field frequency [35]. Figure 4 shows the variation of the aspect ratio with applied field frequency and summarizes the physical mechanisms underlying the observed shape changes.

While the shape of vesicles with conductivity ratio $\Lambda > 1$ is always prolate, if $\Lambda < 1$, that is, the vesicle is filled with a solution less conducting than the suspending one, the

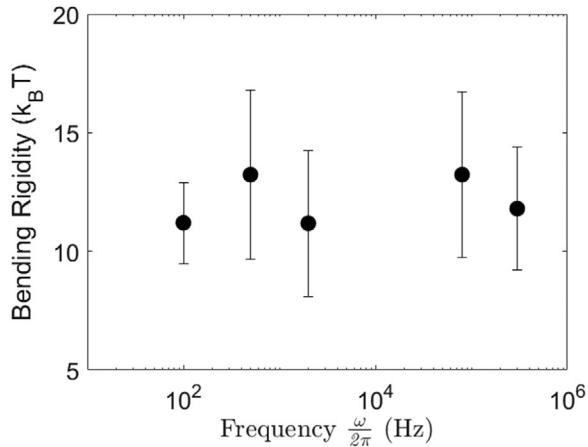


Figure 3. Bending rigidity of a palmitoyloleoylphosphatidylcholine (POPC) lipid bilayer membrane measured at different field frequencies. Solutions contain 0.2 mM NaCl inside ($\lambda_{in} = 42 \mu\text{S}/\text{cm}$) and no salt outside ($\lambda_{ex} = 2 \mu\text{S}/\text{cm}$). Values obtained from population averages over 12–15 vesicles. Field amplitude is increased from 2 to 10 kV/m with steps of 0.5 kV/m.

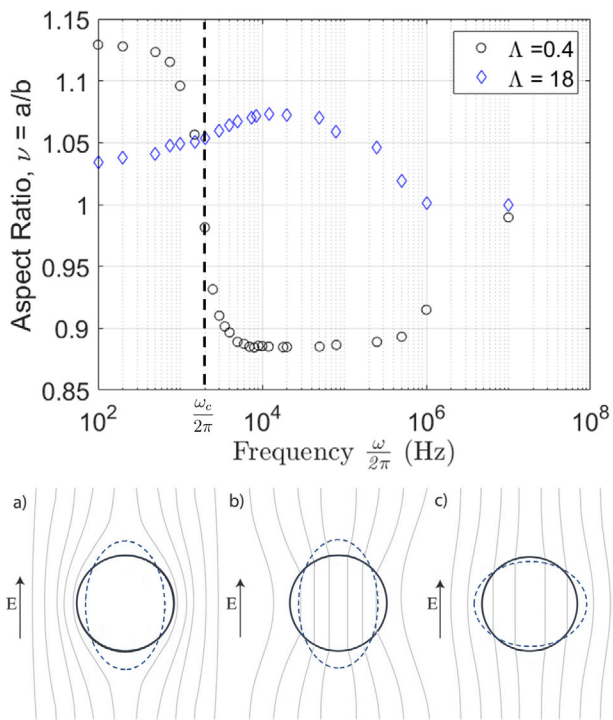


Figure 4. (Top) Deformation of two palmitoyloleoylphosphatidylcholine (POPC) GUVs in a uniform AC electric field with amplitude 6 kV/m at different field frequencies in hertz at different conductivity ratios. (Bottom) Physical mechanisms of the frequency-dependent vesicle shape in an applied uniform AC field. The lines correspond to constant electric field. (A) At low frequencies, $\omega \ll \omega_c$, the membrane capacitor is fully charged and the electric field inside the vesicle is zero. (B and C) At intermediate frequencies, $\omega > \omega_c$, it is short circuited. (B) If the enclosed solution is more conducting than the suspending medium, $\Lambda > 1$, vesicle is pulled into an prolate ellipsoid. (C) The polarization is reversed in the opposite case $\Lambda < 1$ and the vesicle deforms into an oblate ellipsoid.

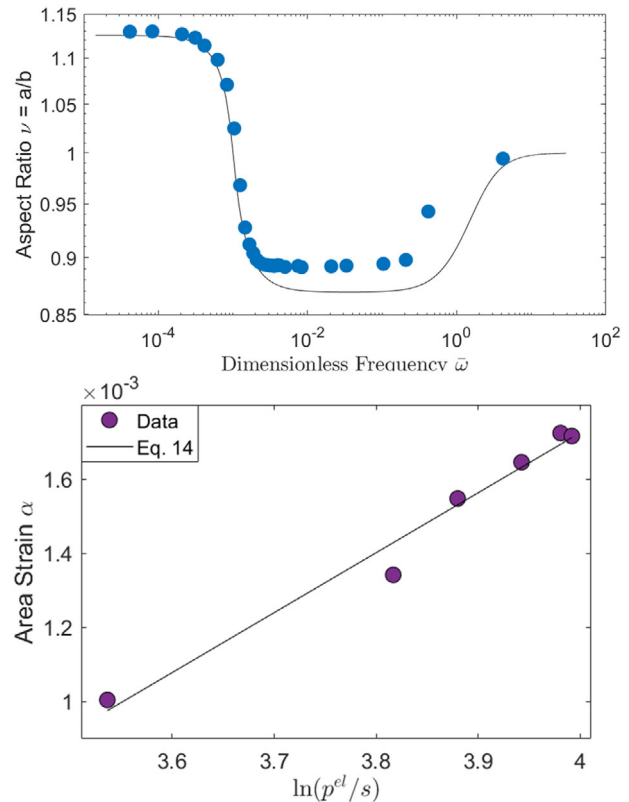


Figure 5. (Top) Frequency dependence of the aspect ratio of the same palmitoyloleoylphosphatidylcholine (POPC) vesicle as in Fig. 2 at $E_0 = 6 \text{ kV}/\text{m}$. The solid line is Eq. (13) with the $\kappa = 12.67 k_B T$ obtained by the classical electrodeformation method and $\sigma_0 = 3.53 \times 10^{-7} \text{ N}/\text{m}$. (Bottom) The fit of frequency-sweep data at $\omega < \omega_c$ yields $\kappa = 14.97 k_B T$ with $R^2 = 0.975$.

deformation parameter $s(\omega)$ is positive at low frequencies indicating prolate deformation, which decreases with frequency and becomes zero at a certain frequency. Above this critical frequency, the shape becomes oblate. For $\tilde{C}_m \gg 1$, a condition that is typically satisfied for membranes, the critical frequency can be approximated as [36]

$$\omega_c = \frac{\lambda_{in}}{RC_m} \frac{1}{\sqrt{(1-\Lambda)(3+\Lambda)}}. \quad (12)$$

Thus, the membrane capacitance can be obtained from the experimentally measured critical frequency for prolate–oblate transition [26, 37]. The frequency-dependent shape is described by

$$s(\bar{\omega}) = \frac{\varepsilon E_0^2 R}{\sigma_0} \frac{p^{el}(\bar{\omega})}{\exp\left(\frac{64\kappa}{5k_B T} s^2(\bar{\omega})\right)}. \quad (13)$$

Figure 5 shows frequency-sweep experimental data for the same vesicle analyzed in Fig. 2. The theoretical curve is obtained using κ deduced from the classical electrodeformation method discussed in Section 3.1. Thus, the frequency sweep confirms the results from the field-amplitude sweep. Furthermore, the frequency sweep itself can be used to

obtain the bending rigidity. Equation (13) can be recast in a form analogous to Eq. (8):

$$\ln \frac{\varepsilon R E_0^2}{\sigma_0} + \ln \frac{p^{\text{el}}(\omega)}{s} = \frac{8\pi\kappa}{k_B T} \left(\frac{8s^2}{5} \right). \quad (14)$$

Fitting the data in the prolate deformation regime ($\omega < \omega_c$) yields a similar value of the bending rigidity as in Fig. 2. Note that using the whole frequency range is not convenient because vesicle shape changes from a prolate to an oblate ellipsoid. We also observe that the tension σ_0 needed to describe the frequency-sweep data is twice the one obtained from the intercept of the linear fit in Fig. 2. The origin of this increase is currently being investigated. The membrane capacitance obtained from the critical frequency ω_c is $0.72 \pm 0.04 \mu\text{Fcm}^{-2}$ from measurements of 13 vesicles. The value is consistent with the previously reported data by Salipante et al. [26]. Note that the capacitance is obtained independent of bending rigidity and tension.

3.3 Apparent bending rigidity of membranes with tubes

Biological membranes are inherently asymmetric [38]. Different lipid compositions in the two leaflets and proteins [39–41], or difference in cytosolic and periplasmic buffer conditions [42], can lead to membrane curvature resulting in formation defects such as tubes [43]. Here we illustrate the utility of the electrodeformation method to measure the bending rigidity and membrane tension of such membranes, as these are difficult to characterize using conventional methods such as flickering spectroscopy [21].

We observe that vesicles with large difference in the salt concentrations inside and outside (filled with 0.5 mM NaCl and suspended in no salt solution) have many tubes with diameter 1–2 μm ; see Fig. 6. The formation of the tubes is likely due to spontaneous curvature arising from asymmetry in the electric double layers adjacent to the membrane. The Debye length (calculated for a 1:1 electrolyte from $\kappa_D = 0.303c^{-1/2}$ nm, where c is the electrolyte concentration in M) is 14 nm for the inner and 78 nm for the outer double layer in the asymmetric case, while in the symmetric case the outer double layer is 10 nm. For the salt-free solution, the procedure to estimate the Debye layer thickness is given in [20].

We measured the bending rigidity using the electrodeformation method and found membranes with tubes to be more rigid ($17.4 \pm 3.3 k_B T$) compared to symmetric membranes ($12.0 \pm 2.2 k_B T$) as shown in Fig. 6.

4 Concluding remarks

We describe a method to characterize the electric and mechanical properties of biomimetic membranes using a uniform AC electric field. The approach relies on the analysis of the variation of the equilibrium shapes of GUVs with electric field amplitude and frequency. Using the theory developed in [25], we derive the theoretical foundations for the

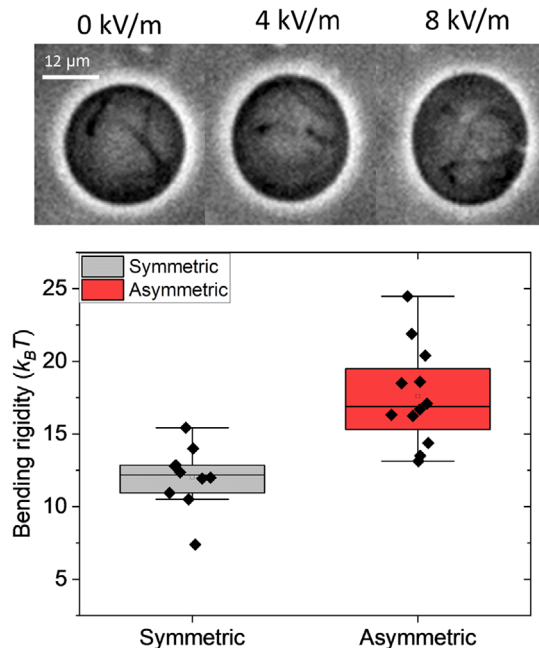


Figure 6. (Top) Snapshots of GUV showing tubes (0.5 mM NaCl inside and no salt outside). (Bottom) Membrane bending rigidity obtained for asymmetric (0.5 mM NaCl and no salt outside) and symmetric (0.5 mM NaCl inside and 0.8 mM NaCl outside) membranes.

method originally proposed by Kummrow and Helfrich [24], which utilizes the variation of the area strain on electric field amplitude at fixed field frequency. We show that fitting the dependence of the area strain on either the field amplitude or frequency yields similar values for the bending rigidity and tension. The frequency sweep, however, also provides the membrane capacitance. The latter is obtained from the frequency at which the vesicle shape changes from prolate to oblate ellipsoid as the frequency is increased. We demonstrate the utility of the method by measuring the mechanical properties of membranes with tubes, which so far could only be analyzed using more complex methods such as micropipette aspiration. Our method can be applied to a variety of membrane compositions, including multicomponent systems containing cholesterol, block copolymers, and asymmetric membranes. The method should even work with membranes containing charged lipids since in AC electric field the charged species do not undergo electrophoresis. The extension of the method to such systems will be investigated in near future.

P. V. and H. F. acknowledge financial support by NIGMS award 1R01GM140461.

The authors have declared no conflict of interest.

5 Data availability statement

The data that support the findings of this study are available from the corresponding author upon reasonable request.

6 References

- [1] Bassereau, P., Jin, R., Baumgart, T., Deserno, M., Dimova, R., Frolov, V. A., Bashkirov, P. V., Grubmuller, H., Jahn, R., Risselada, H. J., Johannes, L., Kozlov, M. M., Lipowsky, R., Pucadyil, T. J., Zeno, W. F., Stachowiak, J. C., Stamou, D., Breuer, A., Lauritsen, L., Simon, C., Sykes, C., Voth, G. A., Weikl, T. R., *J. Phys. D* 2018, **51**, 343001.
- [2] Janmey, P. A., Weitz, D. A., *Trends Biochem. Sci.* 2004, **29**, 364–370.
- [3] Le Roux, A.-L., Quiroga, X., Walani, N., Arroyo, M., Rocasachs, P., *Philos. Trans. R. Soc. B* 2019, **374**, 20180221.
- [4] Sitarska, E., Diz-Muñoz, A., *Curr. Opin. Cell Biol.* 2020, **66**, 11–18.
- [5] Keren, K., *Eur. Biophys. J.* 2011, **40**, 1013.
- [6] Sens, P., Plastino, J., *J. Phys. Condens. Matter* 2015, **27**, 273103.
- [7] Cole, K., *Membranes, ions and impulses*, University of California Press, Berkeley, CA 1968.
- [8] Bean, B., *Nat. Rev. Neurosci.* 2007, **8**, 451–465.
- [9] Brownell, W. E., Spector, A. A., Raphael, R. M., *Annu. Rev. Biomed. Eng.* 2001, **3**, 169–194.
- [10] Quinn, T. A., Kohl, P., Ravens, U., *Prog. Biophys. Mol. Biol.* 2014, **115**, 71–75.
- [11] Dimova, R., Aranda, S., Bezlyepkina, N., Nikolov, V., Riske, K. A., Lipowsky, R., *J. Phys. Condens. Matter* 2006, **18**, S1151–S1176.
- [12] Dimova, R., *Annu. Rev. Biophys.* 2019, **48**, 93–119.
- [13] Dimova, R., Marques, C. (Eds.), *The Giant Vesicle Book*, CRC Press, Boca Raton, FL 2019.
- [14] Dimova, R., *Adv. Coll. Int. Sci.* 2014, **208**, 225–234.
- [15] Brochard, F., Lennon, J. F., *J. Phys.* 1975, **36**, 1035–1047.
- [16] Faucon, J., Mitov, M., Meleard, P., Bivas, I., Bothorek, P., *J. Phys.* 1989, **50**, 2389–2414.
- [17] Pecreaux, J., Dobereiner, H.-G., Prost, J., Joanny, J.-F., Bassereau, P., *Eur. Phys. J. E* 2004, **13**, 277–290.
- [18] Gracia, R. S., Bezlyepkina, N., Knorr, R. L., Lipowsky, R., Dimova, R., *Soft Matter* 2010, **6**, 1472–1482.
- [19] Genova, J., Vitkova, V., Bivas, I., *Phys. Rev. E: Stat. Non-linear Soft Matter Phys.* 2013, **88**, 022707.
- [20] Faizi, H. A., Frey, S. L., Steinkuehler, J., Dimova, R., Vlahovska, P. M., *Soft Matter* 2019, **15**, 6006–6013.
- [21] Faizi, H. A., Reeves, C. J., Georgiev, V. N., Vlahovska, P. M., Dimova, R., *Soft Matter* 2020, **16**, 8996–9001.
- [22] Evans, E., Rawicz, W., *Phys. Rev. Lett.* 1990, **64**, 2094–2097.
- [23] Jacobs, M. L., Faizi, H. A., Peruzzi, J. A., Vlahovska, P. M., Kamat, N. P., *Biophys. J.* 2021, **120**, 2317–2329.
- [24] Kummrow, M., Helfrich, W., *Phys. Rev. A* 1991, **44**, 8356–8360.
- [25] Vlahovska, P. M., Gracia, R. S., Aranda-Espinoza, S., Dimova, R., *Biophys. J.* 2009, **96**, 4789–4803.
- [26] Salipante, P. F., Knorr, R. L., Dimova, R., Vlahovska, P. M., *Soft Matter* 2012, **8**, 3810–3816.
- [27] Salipante, P. F., Vlahovska, P. M., *Soft Matter* 2014, **10**, 3386–3393.
- [28] Faizi, H. A., Dimova, R., Vlahovska, P. M., 2021, arXiv:2103.02106.
- [29] Seifert, U., *Z. Phys. B: Condens. Matter* 1995, **97**, 299–309.
- [30] Vlahovska, P. M., *Adv. Planar Lipid Bilayers Liposomes*. 2010, **12**, 103–146.
- [31] Vlahovska, P. M., *Annu. Rev. Fluid Mech.* 2019, **51**, 305–330.
- [32] Vlahovska, P. M., Misbah, C., in: Dimova, R., Marques, C. (Eds.), *The Giant Vesicle Book*, CRC Press, Boca Raton, FL 2019.
- [33] Angelova, M. I., Dimitrov, D. S., *Faraday Discuss. Chem. Soc.* 1986, **81**, 303–311.
- [34] Seifert, U., *Eur. Phys. J. B* 1999, **8**, 405–415.
- [35] Aranda, S., Riske, K. A., Lipowsky, R., Dimova, R., *Biophys. J.* 2008, **95**, L19–L21.
- [36] Yamamoto, T., Aranda-Espinoza, S., Dimova, R., Lipowsky, R., *Langmuir* 2010, **26**, 12390–12407.
- [37] Vitkova, V., Mitkova, D., Antonova, K., Popkirov, G., Dimova, R., *Colloids Surf. A* 2018, **557**, 51–57.
- [38] Lorent, J. H., Levental, K. R., Ganesan, L., Rivera-Longsworth, G., Sezgin, E., Doktorova, M., Lyman, E., Levental, I., *Nat. Chem. Biol.* 2020, **16**, 644–652.
- [39] Simunovic, M., Lee, K. Y. C., Bassereau, P., *Soft Matter* 2015, **11**, 5030–5036.
- [40] Busch, D. J., Houser, J. R., Hayden, C. C., Sherman, M. B., Lafer, E. M., Stachowiak, J. C., *Nat. Commun.* 2015, **6**, 7875.
- [41] Bhatia, T., Agudo-Canalejo, J., Dimova, R., Lipowsky, R., *ACS Nano* 2018, **12**, 4478–4485.
- [42] Karimi, M., Steinkühler, J., Roy, D., Dasgupta, R., Lipowsky, R., Dimova, R., *Nano Lett.* 2018, **18**, 7816–7821.
- [43] Lipowsky, R., *Faraday Discuss.* 2013, **161**, 305–331.